International Journal of Engineering and Science Invention (IJESI)
ISSN (Online): 2319-6734, ISSN (Print): 2319-6726
www.ijesi.org ||Volume 14 Issue 6 June 2025 || PP 33-44

Wind Load Characteristics of Drop-out Fuses under Strong Wind Conditions

Jin-Peng Xie, Su-Hui Zhang, Jian Gao, Yu-Lin Teng, Yan-Ting Lv, Jin-Hua Wu

(Electric Power Research Institute of State Grid Gansu Electric Power Company, Lanzhou 730070, China)

Abstract: *The wind load characteristics of drop-out fuses under strong wind conditions are investigated using numerical simulation methods. The results indicate that, under the same wind speed, the forces acting along the porcelain insulator axis (y-direction), the metal component insertion direction (x-direction), and the direction perpendicular to the x–y plane (z-direction) increase sequentially. As wind speed increases, both the forces in the x and z directions and the moments around the y and z axes are significantly enhanced. When the wind direction changes, the force in the z direction and the twisting moment around the y-axis exhibit a trend of first increasing and then decreasing with the wind direction angle, while the force in the y direction and the moment around the z-axis show the opposite trend. The load on the drop-out fuses reaches its peak at a wind direction of 90°. Meanwhile, a correlation among the drag coefficient, Reynolds number, and wind direction angle have been established. Additionally, the load on the fuse also varies with the installation angle. The shear stress at the interface between the metal component and the cement mortar increases with wind speed, with its maximum value occurring at wind direction of 90°, which is about one-tenth of the permissible shear stress.*

Keywords - *Drop-out fuses, Porcelain insulator, Shear stress, Wind load*

Date of Submission: 07-06-2025 Date of Acceptance: 17-06-2025

I.INTRODUCTION

Drop-out fuses are the most commonly used short-circuit protection switches for distribution line branches and distribution transformers. They are composed of three parts: porcelain insulators, moving and stationary contacts, and a fuse tube, and are widely used in high-voltage power transmission networks. Drop-out fuses are widely used in high-voltage power transmission networks [1-6]. Porcelain insulators are key components of drop-out fuses. Due to insulation and installation requirements, one end of the metal part is inserted into the porcelain insulator of the drop-out fuse, and the metal part and the porcelain insulator are connected by cement and colloidal materials. In actual use, this connection method between the metal part and the porcelain insulator becomes the weakest link in the strength of the porcelain insulator. Once this connection of the porcelain insulator is damaged, it will cause power outages to the grid or equipment, and may also cause electric shocks and falling parts, resulting in grid accidents. Therefore, the research on the reliability of porcelain insulators plays a key role in the safe operation of the power grid.

The northwestern region of China is vast and sparsely populated, with a relatively harsh natural environment. Its unique geographical location and environment result in strong wind conditions. In areas with strong winds, when the wind speed, wind direction, and installation inclination angle of the drop-out fuse change, the windward area and surface pressure of the drop-out fuse also change. As a result, the forces and moments in three directions acting on the drop-out fuse generate twisting moment at the bonding surface between the porcelain insulator and the metal parts, resulting in shear stress on the surface where the metal parts bond with the cement mortar. Therefore, the connection between porcelain insulators and metal parts is one of the main factors to consider in drop-out fuse design. Research on the wind load characteristics of drop-out fuses can provide a reference for improving the structural safety and reliability of porcelain insulators.

A considerable amount of research has been conducted on the safe operation of drop-out fuses. Wang et al. [7] used experimental methods to analyze the root causes of overheating in drop-out fuses at different operating currents and locations. To address the lack of reliable remote monitoring methods and equipment for fuses, Ju et al. [8] developed a monitoring and alarm device based on the drop characteristics of fuses after a power failure. Sun et al. [9] analyzed the influence of porcelain insulator flange inclination and manufacturing defects on insulator fracture through inspection and measurement tests. The results showed that tensile force, torsion, and manufacturing defects at the weakest point of the porcelain insulator are among the main causes of fracture failure. Li et al. [10] studied the effects of retarder type, cement type, and mineral admixture content on

the strength of porcelain insulator cementing materials through experimental methods, providing a basis for upgrading intelligent production lines for porcelain insulators. Sun et al. [11] found that the inclination of the porcelain insulator support platform surface can cause the center of gravity of the upper insulation casing assembly to shift, and the shear stress generated under the combined action of pressure and tension is one of the main causes of porcelain insulator fracture. Considering the manufacturing process of porcelain insulators, Han et al.[12] used experimental methods to analyze the causes of mud deposition in post insulators and proposed corresponding improvement measures. These studies analyzed the main causes of insulator fracture from aspects such as manufacturing process, installation method, and material type, providing a good reference for their safe operation.

Lei et al. [13] investigated the influence of composite insulator umbrella diameter combinations, incoming wind speed, and direction on the wind pressure distribution on the insulator surface using wind tunnel experiments and finite element simulations. Their findings provide a reference for insulator selection and design in windy areas. Liu [14] employed three methods to calculate and analyze the maximum bending stress and working load on porcelain insulators under different wind speeds, comparing the advantages of each method. Zhou et al. [15] conducted anisotropic and isotropic characteristic value buckling analyses of composite insulator cores using ANSYS finite element software. Their results offer valuable insights for the design and improvement of insulator strings. Liu et al. [16] studied the wind load on a single-unit post insulator under various wind conditions based on computational fluid dynamics and compared the results with those obtained from empirical formulas. The study revealed that empirical formulas tend to overestimate the wind load on single-unit insulators. Ding et al. [17] analyzed the wind load characteristics of insulator strings made of different materials using ABAQUS finite element software. The results indicated that the material of the insulator string has a relatively small impact on conductor galloping. Wang et al. [18] proposed a method for modeling wind fields in mountainous valleys for transmission lines and studied the wind deflection characteristics of insulator strings under the influence of mountain valley winds.

The above research provides a solid foundation for calculating wind loads on porcelain insulators of drop-out fuse. However, they have not focused on the shear stress present at the bonding surface between the metal parts and cement mortar, and therefore have not revealed the wind load characteristics of shear stress. Moreover, these studies have considered relatively low wind speeds and assumed constant wind direction, without quantifying the magnitude of the wind load on the porcelain insulator. In light of this, this paper employs numerical methods based on overset grid technology to investigate the wind load characteristics of drop-out fuses under various wind speeds, directions, and installation angles. The study also examines the characteristics of shear stress induced by wind loads at the bonding surface between the metal parts and cement mortar. This research aims to summarize the wind load characteristics of drop-out fuse under strong wind conditions, providing a reference for the design, load calculation, and installation of drop-out fuses.

II.METHODS

2.1 Drop-out fuse calculation model

As shown in Figure 1(a), the RW-12 10 kV drop-out fuse is used as the research object. Its structural height is 374 mm, the umbrella diameter is 105 mm, and the creepage distance is 372 mm. For the convenience of subsequent numerical modeling, the connecting components such as bolts and springs in the original model have been simplified. The simplified structure is shown in Figure 1(b), where the installation angle is the angle between the fuse tube's axis and the vertical line to the ground.

2.2 Boundary conditions and mesh division

The fluid is simulated by solving the RANS equations using ANSYS FLUENT (2022R1 version), with the RNG k-epsilon turbulence model employed for equation closure. The pressure-velocity coupling utilizes the SIMPLEC algorithm, while the momentum equation, turbulence kinetic energy, and dissipation rate are discretized using second-order upwind scheme. Time discretization is handled with second-order implicit scheme. Convergence is deemed achieved when the residuals reach 10^{-4} and the loads on the drop-out fuse exhibit periodic behavior. To minimize the influence of the blocking effect of the computational domain boundary on the results, the dimensions of the flow field computational domain are set to be more than 4 times the structural dimensions of the drop-out fuse in the corresponding directions. The schematic diagram of the computational domain is shown in Figure 2(a). In the diagram, surface A has an area of 1.5 m × 1.5 m. The inlet velocities applied to this surface are 25, 30, 35, 40, and 45 m/s, respectively. The turbulence intensity is set to 5% of the kinetic energy of the fluid flow, and the turbulent viscosity ratio is 10. The air density is taken as 1.225 kg/m³. Surface B is the pressure outlet, with a pressure set at 0 Pa, and other surrounding walls are slip walls (without normal mass flux). The drop-out fuse is located 1.5 m from the inlet. The coordinate system of the drop-out fuse is shown in Figure 2(b), where the origin is located at the center of the connection between the

porcelain insulator and the metal part. The *x*-axis is parallel to the metal part and points towards the fuse tube, the *y*-axis is parallel to the center line of the porcelain insulator and points vertically upwards, and the *z*-axis is perpendicular to both the *x*-axis and *y*-axis.

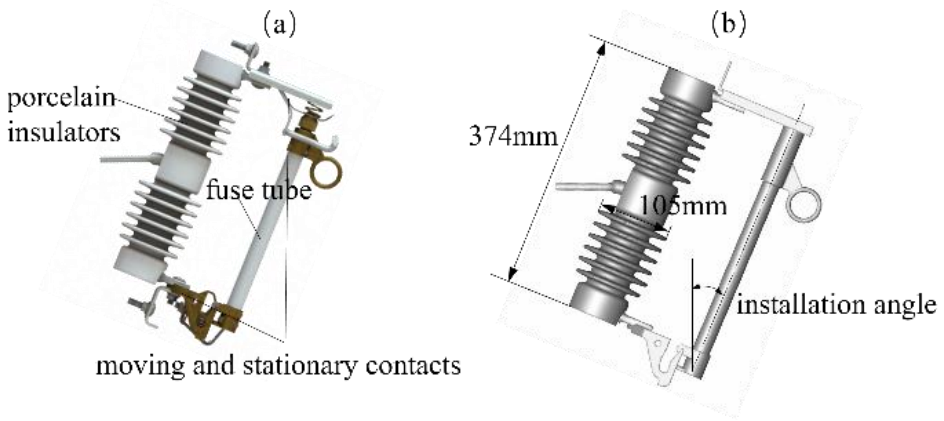

Figure 1. *Drop-out fuse model: (a) Original model; (b) Simplified model*

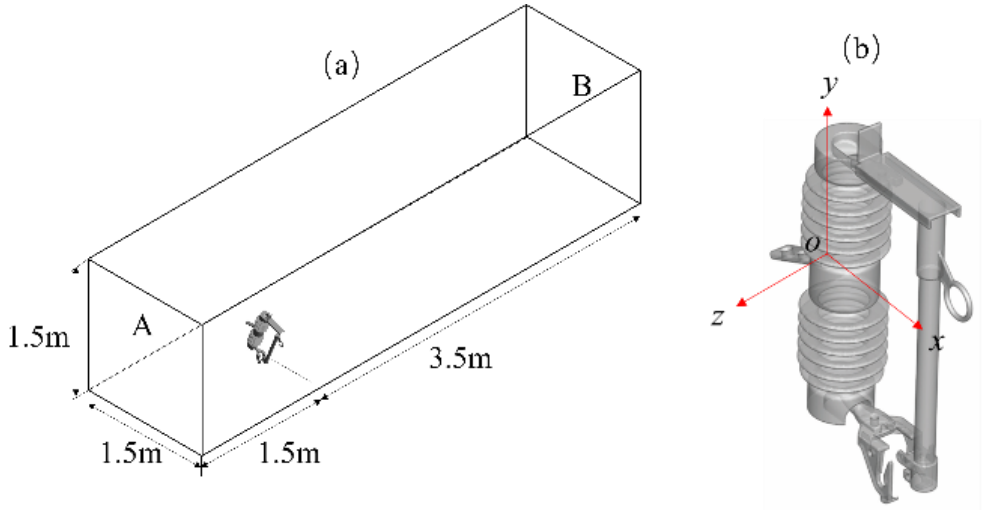

Figure 2. *Schematic diagram of the (a) Computation domain and (b) Drop-out fuse coordinate system.*

To facilitate the study of the impact of wind direction and installation angle on the wind load characteristics of the drop-out fuse, and to reduce the workload of mesh generation, the overlapping grid technique reported by Jia et al. [19] was used during mesh division. The overlapping grid consists of a background grid and component grid, which have the advantage of clear data transmission and are beneficial for generating meshes for moving components.

When the overlapping grid technique is used, the process begins with the "hole-cutting" technique to identify the coverage and shielding regions of each sub-grid. Nodes in the overlapping area covered by the primary grid are masked, while interpolation nodes are positioned at the interfaces between different sub-grids. Subsequently, the system employs a weighted interpolation algorithm to transfer physical quantities between donor cells and receptor cells, ensuring both continuity and conservation within the overlapping regions. This approach guarantees the numerical stability and fidelity of multidomain solutions in simulations involving complex geometries or moving boundaries.

The entire cuboid computational domain is set as the background grid, while the grid surrounding the drop-out fuse is the component grid. The overlapping area between the background grid and the component grid is designated as the grid overlap region.

Due to the complex geometry of the porcelain insulator, mesh refinement is performed on the surface of the drop-out fuse to capture the influence of structural changes on the flow field characteristics. Figure 3(a) and (b) show the schematic diagram of the mesh distribution on the surface and around the drop-out fuse. After mesh independence verification, the total amount of mesh in the computational domain was finally determined to be approximately 5.5 million. Figure 3(c) shows the schematic diagram of the incoming flow direction for the

drop-out fuse. In subsequent studies, when it is necessary to alter the incoming wind direction, it merely requires rotating the component grid surrounding the drop-out fuse.

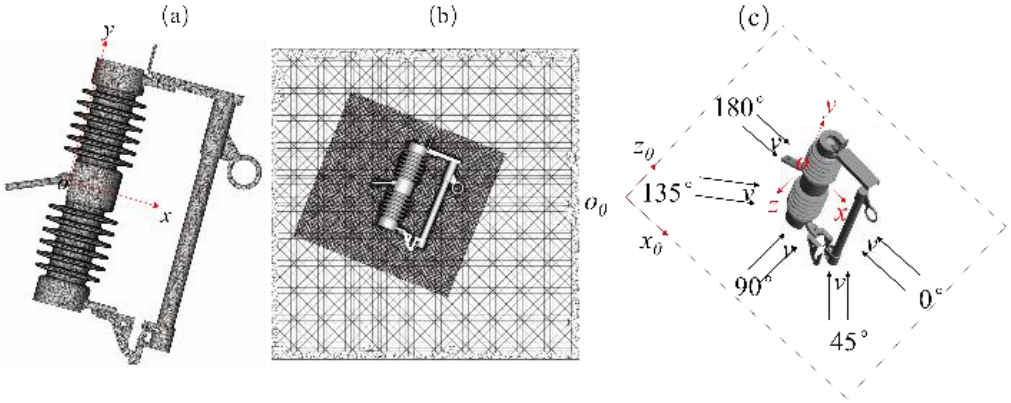

Figure 3. *Mesh distribution and incoming wind direction schematic: (a) Mesh distribution on the surface of the drop-out fuse; (b) Mesh distribution around the drop-out fuse; (c)Incoming wind direction schematic.*

III.RESULTS AND DISCUSSIONS

3.1 Influence of the wind speed on wind load of drop-out fuses

When the installation angle of the drop-out fuse is fixed and the incoming wind direction remains unchanged, variations in wind speed can cause changes in the wind load on the drop-out fuse. When the installation angle of the drop-out fuse is 22° and the incoming wind direction is 90°, as illustrated in the wind direction schematic diagram in Figure 3(c), and the incoming wind speeds are 25, 30, 35, 40, and 45 m/s, the wind load characteristics on the drop-out fuse are analyzed.

Figure 4(a) shows the variation of the forces F_x, F_y, and F_z that the drop-out fuse experiences in the x, y, and z directions as wind speed changes. The relevant data are directly extracted from the post-processing software of ANSYS FLUENT. As the figure indicates, with an increase in incoming wind speed, the forces F_x and F_z in the x and z directions on the drop-out fuse gradually increase. When the incoming wind speed increases from 25 m/s to 45 m/s, the forces in the x and z directions (F_x and F_z) on the drop-out fuse increase by 2.53 and 2.27 times, respectively. Additionally, at the same incoming wind speed, the components of force in the y, x, and z directions (F_y, F_x, and F_z) increase sequentially.

When wind passes through the drop-out fuse, due to the different wind pressures acting at different positions, the drop-out fuse will generate twisting moments. Figure 4(b) illustrates the variation of twisting moments around the center of the connection between the metal part and the porcelain insulator at different wind speeds. Here, M_x represents the twisting moment around the x-axis, M_y around the y-axis, and M_z around the z-axis. The figure shows that as wind speed increases, the twisting moments M_y around the y-axis and M_z around the z-axis gradually increase. This is because the wind pressure difference on the surface of the drop-out fuse in the z and x directions increases with wind speed. When the incoming wind speed increases from 25 m/s to 45 m/s, M_x changes slightly, while M_y and M_z increase by 2.26 times and 0.74 times, respectively. At the same wind speed, the twisting moments around the x-axis, z-axis, and y-axis increase sequentially.

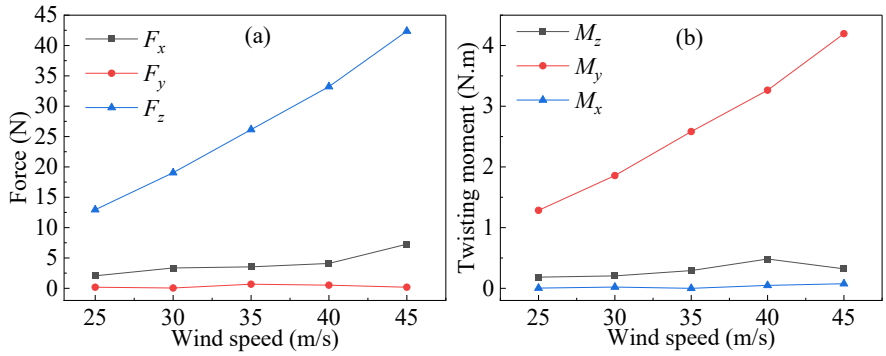

Figure 4. *Variation of forces and twisting moment on drop-out fuse with wind speed at 90° wind direction and 22° installation angle: (a) Force; (b) Twisting moment. The loads of the drop-out fuse shown in the figure are the absolute values of the actual loads.*

Figure 5 shows the surface pressure distribution of the drop-out fuse under different wind speeds. The figure indicates that the highest positive pressure occurs at the windward edge of the insulator's umbrella skirt and the windward side of the fuse tube, while the greatest negative pressure occurs between the umbrella skirts on the sides of the insulator and on the side of the fuse tube exposed to crosswinds. As wind speed increases, the magnitude of both positive and negative pressures gradually increases. When the wind speed increases from 25 m/s to 45 m/s, the magnitude of positive pressure increases from approximately 400 Pa to 1300 Pa, while the magnitude of negative pressure increases from approximately 1700 Pa to 5600 Pa. Therefore, at the same wind speed, the pressure differences in the y, x, and z directions on the drop-out fuse increase sequentially. With increasing wind speed, the forces F_x in the x direction and F_z in the z direction on the drop-out fuse gradually increase.

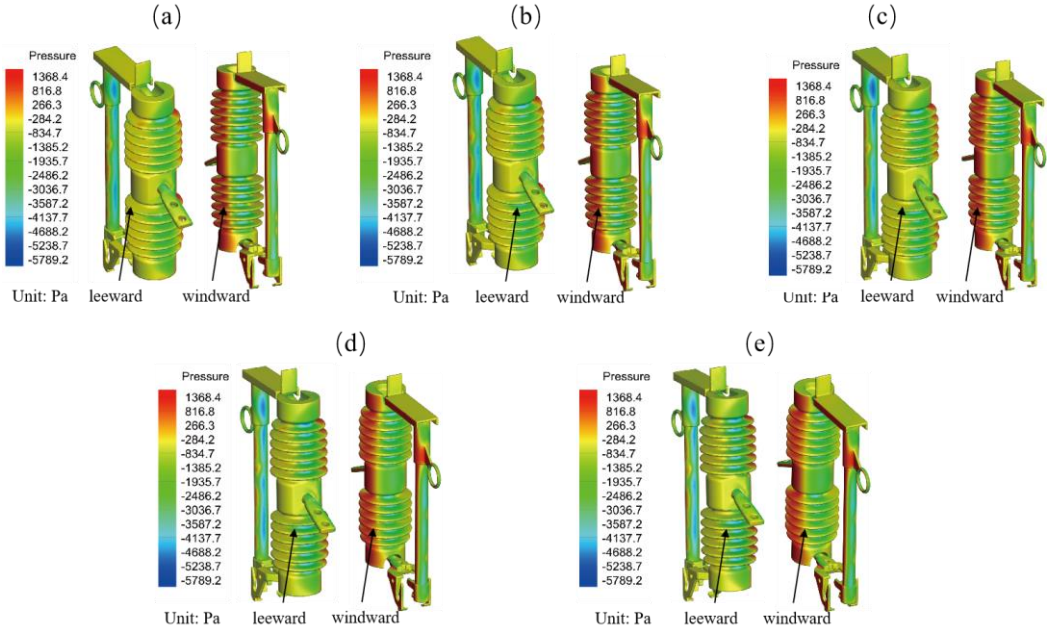

Figure 5. *Variation of the surface pressure distribution on the drop-out fuse with wind speed at 90 ° wind direction and 22 ° installation angle: (a) 25m/s; (b) 30m/s; (c) 35m/s; (d) 40m/s; (e) 45m/s.*

3.2 Influence of the wind direction on wind load of drop-out fuses

When wind passes through the drop-out fuse, the wind around the porcelain insulator and fuse tube interferes with each other. Therefore, when the wind direction changes, the wind load characteristics of the drop-out fuse will also change. When the installation angle of the drop-out fuse is 22°, and the incoming wind speed is 45 m/s at wind directions of 0°, 45°, 90°, 135°, and 180°, as shown in Figure 3(c), the impact of wind direction on the wind load of the drop-out fuse is analyzed.

Figure 6(a) shows the variation of the forces F_x, F_y, and F_z on the drop-out fuse in the x, y, and z directions with changes in wind direction. The figure indicates that the force F_z in the z direction increases and then decreases as the wind direction increases, reaching a maximum at 90° incoming wind direction and relatively smaller at 0° and 180°. This is because, at 90°, the windward area of the drop-out fuse in the z direction is the largest, while at 0° and 180°, the windward area is relatively smaller. When the wind direction changes, the maximum value of the force F_z in the z direction increases 16.7 times compared to the minimum value. The force F_y in the y direction shows a decreasing and then increasing trend with wind direction, reaching a minimum at 90° and relatively larger at 0° and 180°. This trend is due to the smallest windward area in the y direction at 90° compared to a relatively larger area at 0° and 180°. As the wind direction changes, the maximum value of the force F_y in the y direction increases 81.6 times compared to the minimum value.

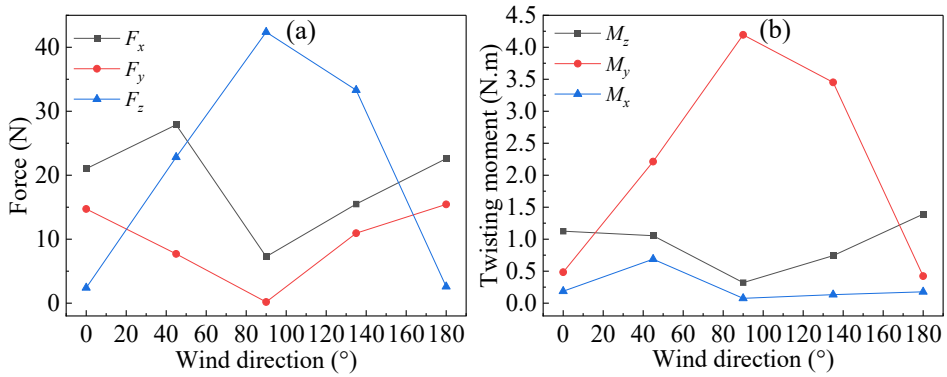

Figure 6. *Variation of the forces and the twisting moments acted on drop-out fuse with wind direction at 45m/s wind speed and 22 ° installation angle:(a) Force; (b) Twisting moment. The loads of the drop-out fuse shown in the figure are the absolute values of the actual loads.*

Figure 6(b) shows the changes in twisting moments around the center of the connection between the metal part and the porcelain insulator under different wind directions. With increasing wind direction, the twisting moment around the *y*-axis initially increases and then decreases, reaching its maximum at 90°. This occurs because the windward area of the drop-out fuse in the *z* direction increases and then decreases with wind direction. When the wind direction changes, the maximum twisting moment around the *y*-axis increases 8.9 times compared to the minimum value. The twisting moment around the *z*-axis shows a decreasing and then increasing trend, reaching a minimum at 90°, as the windward area in the *x* direction initially decreases and then increases with wind direction. As the wind direction changes, the maximum twisting moment around the *z*-axis increases 3.3 times compared to the minimum value. Therefore, when installing drop-out fuses, the impact of wind direction changes on the wind load should be considered.

Figure 7 shows the cross-sectional velocity streamlines of the drop-out fuse under different wind directions, it is evident that apart from the 90° direction, other wind directions result in significant interference between the porcelain insulator and the fuse tube. The downstream components are affected by the wake from upstream components, causing surface pressure changes on the porcelain insulator and fuse tube. Therefore, at 90°, the forces F_x in the *x* direction and F_y in the *y* direction are minimized.

3.3 Influence of the installation angle on wind load of drop-out fuses

When installing a drop-out fuse, it is essential to ensure that when the fuse melts, the circuit can be disconnected by the weight of the fuse tube. This requires determining a reasonable installation angle (the angle between the fuse tube's axis and vertical line to the ground). Typically, the installation angle ranges from 15° to 30°.

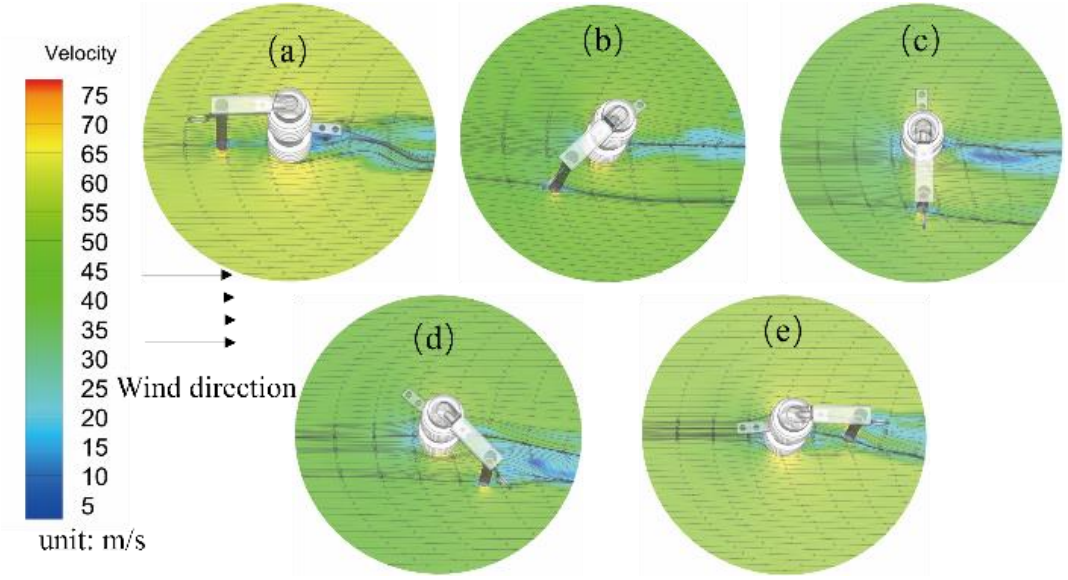

Figure 7. *Cross-sectional velocity streamline of the drop-out fuse at different wind directions with a wind speed of 45 m/s and a 22 ° installation angle: (a) 0°; (b) 45°; (c) 90°; (d) 135°; (e) 180°*

Figure 8 illustrates the changes in force and twisting moment experienced by the drop-out fuse under a wind speed of 45 m/s and a wind direction of 180° when the installation angles are 15°, 18°, 22°, 26°, and 30°. As shown in Figure 8(a), when the installation angle increases from 15° to 30°, the force in the x direction (F_x) of the drop-out fuse changes slightly, while the forces in the y and z directions (F_y and F_z) change significantly. Compared to the minimum values, the maximum value of the force in the x direction increases by 11.6%, while the maximum values of the forces in the y and z directions increase by 1.5 times and 9.5 times, respectively. By comparing the forces on the drop-out fuse at different installation angles, it can be observed that when the installation angle is 30°, the forces in all three directions reach their maximum values.

As shown in Figure 8(b), as the installation angle increases, the twisting moment around the z-axis gradually increases, while the twisting moments around the x-axis and z-axis exhibit significant fluctuations, reaching their maximum values at higher installation angles. Compared to the minimum values, the maximum twisting moments around the x-axis, y-axis, and z-axis increase by 5.2 times, 8.9 times, and 1.4 times, respectively.

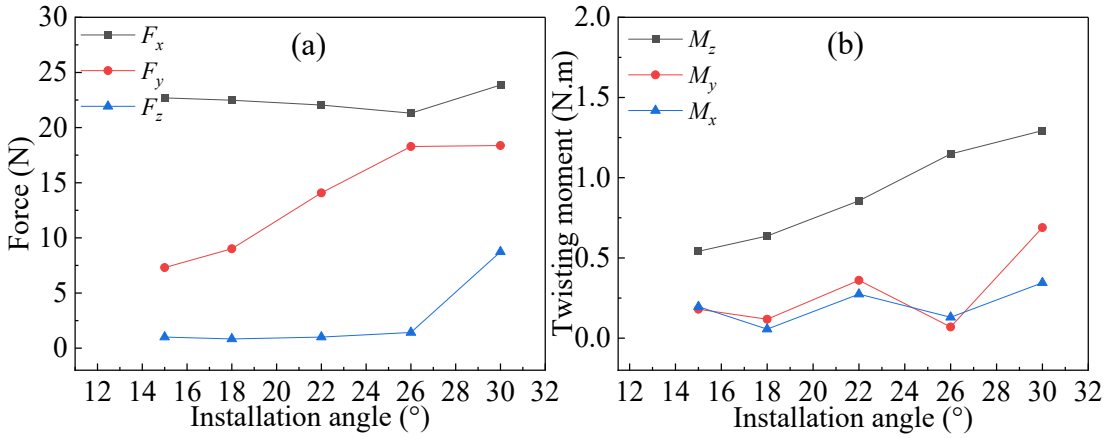

Figure 8. *Variation of the forces and twisting moments acted on drop-out fuse with installation angle at 45m/s wind speed and 180 ° wind direction: (a) Force; (b) Twisting moment. The loads of the drop-out fuse shown in the figure are the absolute values of the actual loads.*

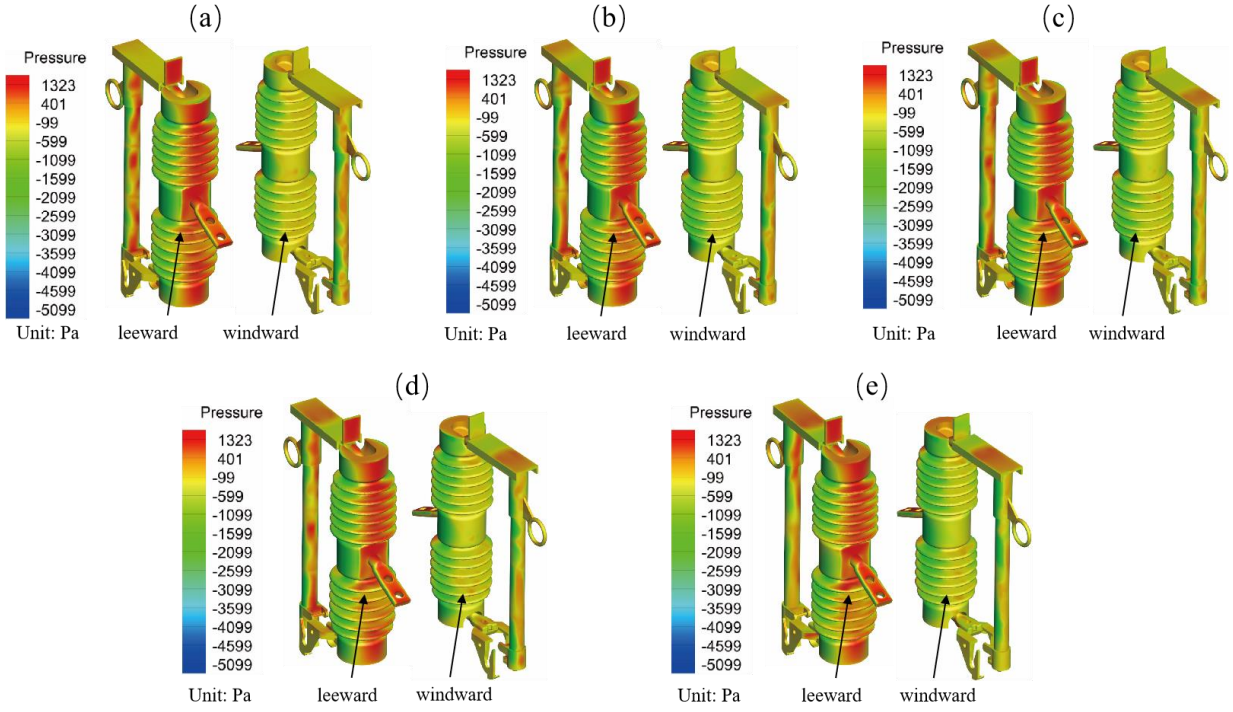

Figure 9. *Variation of the surface pressure distribution on the drop-out fuse with installation angle at 45m/s wind speed and 180 ° wind direction: (a) 15°; (b) 18°; (c) 22°; (d) 26°; (e) 30°*

As shown in Figure 9 depicting the surface pressure distribution of the drop-out fuse at different installation angles, under the conditions of 45 m/s incoming wind speed and 180° wind direction, the surface pressure amplitude of the drop-out fuse varies with installation angle due to changes in its windward area and aerodynamic profile. At 30° installation angle, the maximum pressure differential reaches its peak value. This results in variations of the force and moment loads on the drop-out fuse (as shown in Figure 8) with installation angle, which also attains maximum values at 30°. Therefore, during practical installation of drop-out fuses, the impact of installation angle variations on wind load should be considered, and it is recommended that the installation angle not exceed 26°.

3.4 Relationship between Reynolds number and drag coefficient

As revealed by the above studies, under certain conditions, the square of the incoming wind speed is not proportional to the flow direction drag experienced by the drop-out fuse. This indicates that when the inflow parameters and the windward orientation of the drop-out fuse change, the airflow state around the fuse might also change. To analyze this phenomenon, the relationship between the Reynolds number (*Re*) and the drag coefficient (C_d) in the flow direction for the drop-out fuse is examined. In the calculation of *Re*, the characteristic length (*de*) is defined as follows:

$$de = 4V / S \tag{1}$$

where V=0.007 m^3 is the volume of the drop-out fuse, and S=0.331 m^2 represents its surface area.

The Reynolds number can be expressed as:

$$Re = vd_e / \upsilon \tag{2}$$

where v is the incoming wind speed and v is the kinematic viscosity of the fluid.

The drag coefficient is defined as:

$$C_d = F_{z_0} / (0.5\rho v^2 A) \tag{3}$$

where F_{z0} is the drag force on the drop-out fuse in the inflow direction, resolved from the component F_x, F_y, and F_z in the inflow direction (the z_0-direction in Figure 3); ρ is the fluid density; v is the kinematic viscosity of the fluid; and A is the projected area of the drop-out fuse.

Figure 10 shows the relationship between the Reynolds number variations caused by changes in wind speed under different wind directions and the drag coefficient of the drop-out fuse in the flow direction. As can be seen from the figure, the drag coefficient exhibits minor variations with the Reynolds number under the same wind direction condition.

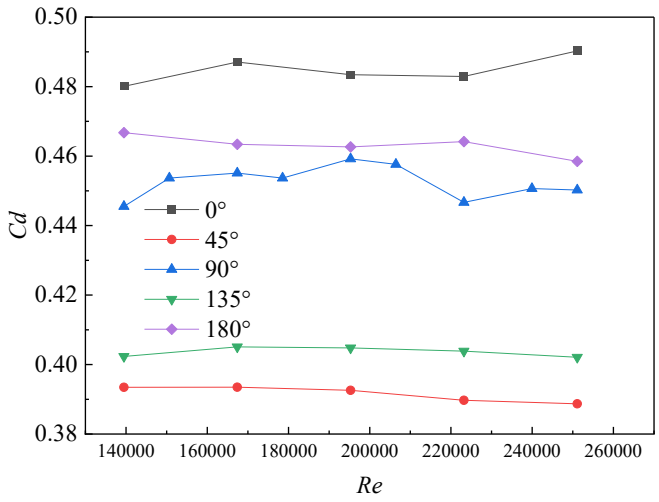

Figure 10. *Relationship between Reynolds number and drag coefficient under different wind directions.*

Based on the data of drag coefficients, Reynolds number, and wind direction angle under multiple wind directions, a multiple nonlinear regression method is used to fit the relationship between the drag coefficient, Reynolds number, and wind direction angle. Considering fluid dynamics characteristics, the initial model included logarithmic terms of the Reynolds number, first and second order trigonometric terms of the wind direction angle, as well as interaction terms. After optimization using the least squares method and evaluating the significance of each coefficient, the resulting fitting expression is:

$$C_d = 0.46 - 0.007.\ln\left(\frac{Re}{200000}\right) - 0.033.\sin\theta + 0.03.\cos\theta + 0.04.\sin 2\theta \tag{4}$$

where θ is the wind direction angle, with units of radians.

To verify the validity of the parameter relationships described above, the drag coefficients obtained from numerical calculations were compared with those predicted by Equation (4), as shown in Figure 11. The black solid line in the figure represents the ideal fitting line, indicating perfect agreement between the numerical results and the model predictions. The red dashed lines denote the bounds of ±5% relative error. As can be seen, the relative errors of most predicted drag coefficients are within ±5%, with an average relative error of −2.59% and a maximum relative error of −5.05%, which fully demonstrates the accuracy of the model.

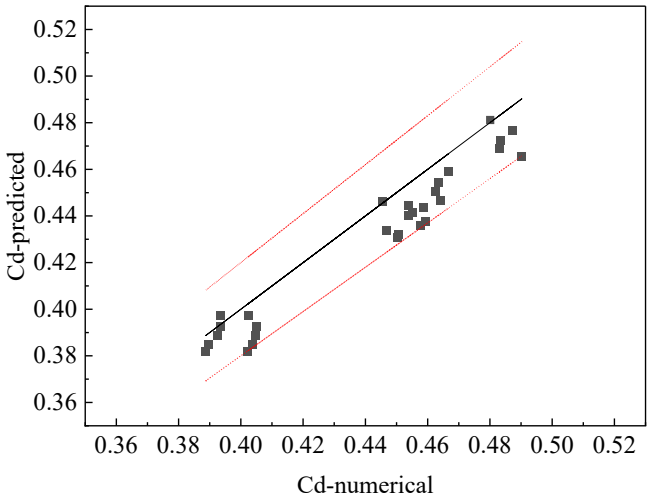

Figure 11. *Comparison of drag coefficients obtained from numerical calculations and model predictions.*

3.5 Shear stress analysis of the drop-out fuse

Gao et al. [20] observed through experiments that the mechanical failure of porcelain insulators invariably occurs at the joint between the porcelain insulator, cementing agent, and metal fitting. Therefore, a reliable connection between the metal parts and the porcelain insulator is fundamental to ensuring the safe operation of drop-out fuses.

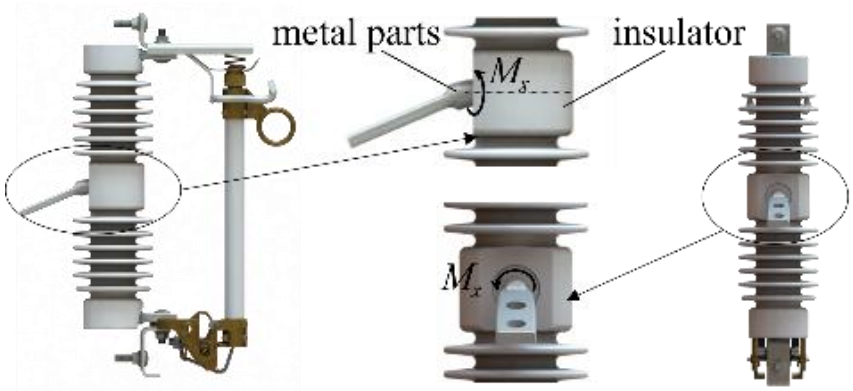

Figure 12. *Connection relationship between metal parts and porcelain insulators and schematic diagram of twisting moment.*

Figure 12 shows the connection relationship between the metal parts and porcelain insulators, as well as the schematic diagram of the twisting moment. Currently, in the production of porcelain insulators, a cementing process is employed to bond the porcelain insulator and metal parts together using a cementing agent, enabling the insulator to achieve the desired supporting and insulating effects in power transmission and transformation systems [21]. Various types of cementing agents are used in this process, including metallic, cement, and sulfur-based agents. Among these, cement-based agents are widely used in porcelain insulator production due to their abundant availability, low cost, and simple application process.

The reliable connection between the metal parts and porcelain insulators is the foundation for ensuring the safe operation of drop-out fuses. At the connection point between the metal parts and porcelain insulators, the twisting moment generated by wind load can cause shear stress at the bonding surface between the metal parts and cement mortar. When the shear stress exceeds the allowable stress, failure will occur at the connection point, leading to a malfunction of the drop-out fuse.

The magnitude of the average shear stress generated at the bonding inter surface between the metal part and the cement mortar is:

$$\tau_{up} = M_{x,up} / Ar \tag{5}$$

$$\tau_{down} = M_{x,down} / Ar \tag{6}$$

$$A = \pi rl \tag{7}$$

where τ_{up} and τ_{down} represent the averaged shear stresses generated at the interface between the metal components and cement mortar due to wind loads on the upper and lower halves of the drop-out fuse porcelain insulator, respectively. $M_{x,up}$ and $M_{x,down}$ represent the twisting moment around the x-axis on the upper and lower halves of the drop-out fuse porcelain insulator, respectively. A is half of the contact area between the metal part and cement mortar of the porcelain insulator. The contact length, l, is 0.04 m, and the radius of the metal part, r, is 0.009 m.

Figure 13 illustrates the variation of the shear stress at the interface between the metal component and cement mortar on the upper and lower halves of the drop-out fuse porcelain insulator under different wind speeds, wind directions, and installation angles.

As shown in Figure 13(a), the shear stresses generated by the upper and lower halves of the insulator at the interface are in opposite directions. With increasing wind speed, both shear stresses gradually increase due to the change in pressure on the surface of the drop-out fuse insulator. When the wind speed increases from 25 m/s to 45 m/s, both shear stresses increase by a factor of 2.3.

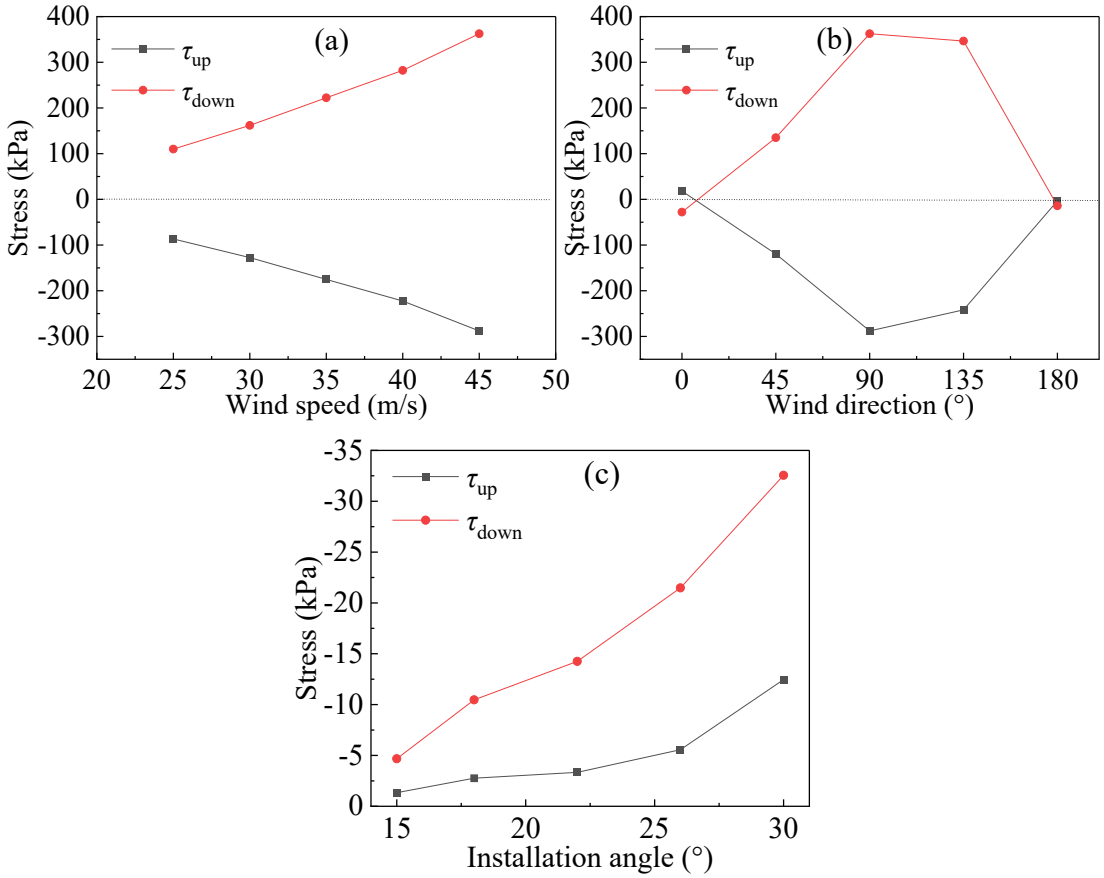

Figure 13. *Variation of the shear stress vs (a) Wind speed at 90 ° wind direction and 22 ° installation angle; (b)Wind direction at 45m/s wind speed and 22 ° installation angle; (c)Installation angle at 45m/s wind speed and 180°wind direction.*

Figure 13(b) shows that the directions of the shear stresses generated by the upper and lower halves of the insulator under 0° and 180° wind directions are different from those under other wind directions. This is due to the increased interference between the drop-out fuse porcelain insulator and the fuse tube under 0° and 180° wind directions. The shear stress at the interface is minimal at a wind direction of 180° and maximal at 90°. The shear stress generated by the upper half of the insulator at 90° is 85 times that at 180°, and the shear stress generated by the lower half is 24 times that at 180°. The maximum shear stress is about 0.360 MPa.

Figure 13(c) demonstrates that the shear stress generated by the upper and lower halves of the insulator increase significantly with larger installation angles. When the installation angle increases from 15° to 30°, the shear stresses in the upper and lower halves amplify by factors of 5.8 and 6.9, respectively. This phenomenon is driven by the proportional increase in torque about the *x*-axis of the drop-out fuse under identical wind speed and direction conditions as the installation angle grows.

The average shear stress at the interface of the metal component and cement mortar is about one tenth of the permissible shear stress. But this shear stress is an averaged one, the maximum shear stress value may be larger than the averaged one, also this shear stress is a time dependent stress due to that wind is time dependent. The interface of the metal component and cement mortar is acted by such dynamic stress, the fatigue failure might occur in the interface. The failure may occur first at the position with the maximum shear stress, then the bounding area at the interface might decrease, and shear stress increases, the fatigue failure may become more serious. Therefore, it is crucial to pay attention to the shear stress at the interface of the metal component and cement mortar.

IV. CONCLUSION

The study employs numerical methods based on overlapping grid technology to analyze the wind load characteristics of the drop-out fuses and the shear stress characteristics on the bonding surface between metal parts and cement mortar under various wind speeds, wind directions, and installation angles. The following conclusions are drawn:

When the wind speed increases from 25 m/s to 45 m/s, the resultant forces on the drop-out fuse in the *x* and *z* directions increase by 2.53 and 2.27 times, respectively. The twisting moments around the *y*-axis and *z*-axis increase by 2.26 times and 0.74 times, respectively. At the same incoming wind speed, the twisting moments around the *x*-axis, *z*-axis, and *y*-axis increase sequentially for the drop-out fuse. When the wind direction changes, the resultant force on the drop-out fuse in the *z*-direction and the twisting moment around the *y*-axis first increase and then decrease with the increase of wind direction. Compared to the minimum values, the maximum values of the *z*-directional force and the twisting moment around the *y*-axis increase by 16.7 and 8.9 times, respectively. Conversely, the resultant force in the *y*-direction and the twisting moment around the *z*-axis first decrease and then increase as the wind direction increases. Compared to the minimum values, the maximum values of the *y*-directional force and the twisting moment around the *z*-axis increase by 81.6 and 3.3 times, respectively. Therefore, in the calculation of wind loads on the drop-out fuse, the impact of wind direction changes on the results should be considered.

When the installation angle increases from 15° to 30°, the force in the x direction (F_x) of the drop-out fuse changes slightly, while the forces in the y and *z* directions (F_y and F_z) change significantly. Compared to the minimum values, the maximum value of the force in the *x* direction increases by 11.6%, while the maximum values of the forces in the *y* and *z* directions increase by 1.5 times and 9.5 times, respectively. The twisting moment around the *z*-axis gradually increases, while the twisting moments around the *x*-axis and *z*-axis exhibit significant fluctuations, reaching their maximum values at higher installation angles. Compared to the minimum values, the maximum twisting moments around the *x*-axis, *y*-axis, and *z*-axis increase by 5.2 times, 8.9 times, and 1.4 times, respectively. Therefore, during practical installation of drop-out fuses, the impact of installation angle variations on wind load should be considered, and it is recommended that the installation angle not exceed 26°.

A nonlinear fitting is conducted on the relationship between the drag coefficient of the drop-out fuse, Reynolds number, and wind direction angle, resulting in a correlation, which reveals a complex interaction between these parameters.

The shear stress at the interface between metal parts and cement mortar varies with wind speed, wind direction, and installation angle. The maximum shear stress occurs at 90° incoming wind direction, and its maximum value is about one tenth of the permissible shear stress. To minimize shear stress caused by wind loads, the drop-out fuse should be installed at 180° wind direction.

This study only considered the influence of average wind characteristics on the load of drop-out fuses. Future research will focus on analyzing the wind load characteristics of drop-out fuses under fluctuating wind characteristics and extreme wind conditions.

ACKNOWLEDGEMENTS

This research was funded by Research Project of State Grid Gansu Electric Power Company Technology Project "Research on Detection Technology, Condition Assessment, and Quality Improvement of Drop-out Fuses in Strong Wind and Large Temperature Difference Areas in Northwest China ", grant number 52272223004M.

REFERENCES

[1] C. Lothongkam, T. Patcharoen & S. Yoomak, Effect of the drop out fuse connection scheme on the overvoltage and the surge arrester in a distribution system. *Energy Reports, 9*, 2023, 41-47.

[2] X. Y. Li, F. M. Wang, H. Cheng, Y. Y. Jin, B. Li & B. H. Geng, Analysis of material and temperature rise test of 10 kV drop-out fuse. *5th IEEE International Conference on Power and Renewable Energy (ICPRE2020)*, Shanghai China, 2020, 328-332.

[3] Y. Y. Jin, F. M. Wang, H. Cheng, X. Y. Li, B. Li & B. H. Geng, Characteristic analysis and test method of pre-arc Seconds characteristic of 12kV drop-out fuse. *5th IEEE International Conference on Power and Renewable Energy (ICPRE2020)*, Shanghai China, 2020, 523-527.

[4] Y. Li, T. Li, H. Chen & Li, X.. Design of intelligent monitoring and management software for Taiwan-level drop-out fuse. *10th IEEE Joint International Information Technology and Artificial Intelligence Conference (ITAIC)*, Chongqing China, 2022, 1528-1531.

[5] X. Liu, C. Pan & Y. Chen, Virtual constraint force control for teleoperation system of live-power line maintenance. *9th IEEE Data Driven Control and Learning Systems Conference (DDCLS*), Liuzhou China, 2020, 906-911.

[6] C. Gong, D. Ye & R. Xie, Development of a HoloLens mixed reality training system for drop-out fuse operation. In emerging trends in intelligent and interactive systems and applications: *Proceedings of the 5th International Conference on Intelligent, Interactive Systems and Applications (IISA2020)*, Shanghai China, 2021, 469-476.

[7] F. M. Wang, Q. Zhao, Y. S. Zhao, et al. Analysis of material and temperature rise test of 10 kV drop-out fuse. *High Voltage Apparatus, 55 (01)*, 2019, 80-86.

[8] Z. Ju, W. Xing, W. Duan, H Sun, X. Sun & S. Liu, Research on status monitoring and fault alarm device of drop-out fuse. *Journal of Physics: Conference Series, 1952(3)*, 2021, 032084.

[9] Q. F. Sun, L. Wang, J. Fu, R.W. Zhang, Y.T. Zhou, & W.J. Zou, Fracture caused by uneven end face of porcelain insulator supporting platform. Insulators and Surge Arresters, (03), 2023, 183-188.

[10] R.K. Li, Z. P. Chen & J. F. Zhou, Research report on insulator cement adhesives for Zhong Cai electric porcelain. *Cement Engineering, 43 (01)*, 2023, 63-67+72.

[11] Q. F. Sun, W. G. Zhang, R. Y. Meng, J. He, Y. Chen & J.Z. Lei, Analysis of fracture of operating ceramic insulators during the process of opening together. *Qinghai Electric Power, 43 (01)*, 2024, 63-67+72.

[12] Y. M. Han, Y. N. Luan, Y.P. Li, X.R.Zhang & J. L.Wu, Analysis and improvement of slurry settling of UHV rod post porcelain insulator. *Insulators and Surge Arresters, (03)*, 2024, 186-192.

[13] Y. Z. Lei, Z. D. Jia, L. H. Zhao, Z. Y. Zhu, Y. Wang, Y. Deng & T. Deng, Study on the distribution of wind pressure of composite insulators and the testing method of anti-wind performance. *Proceedings of the CSEE, 36(9)*, 2016, 2545-2554.

[14] X. J. Liu, Bending stress calculation for porcelain post insulator under wind load. *Insulators and Surge Arresters, (05)*, 2018, 178-184+190.

[15] C. Zhou, R. J. Qin & X. M. Rui, Analysis of mechanical properties of V-shaped insulator string under wind load. *Journal of Engineering Design, 51 (05)*, 2021, 83-88+94.

[16] X. J. Liu & T. Feng, Wind load calculation of post insulator in disconnecting switch. *High Voltage Apparatus, 51 (05)*, 2015, 83-88+94.

[17] S. L. Ding, G. X. Ming, J. H. Shao, H. P. Yang, M. Q. Cai, & L. S. Zhou, Numerical simulation of insulator strings made of different materials under wind load. *Journal of Chengdu University (Natural Science Edition), 43 (02)*, 2024, 166-171.

[18] F. Wang, L. Z. Le & C. X. Song, Study on the wind deflection characteristics of insulator strings under the attack of mountain canyon wind. *Journal of China Three Gorges University (Natural Sciences), 45 (06)*, 2023, 83-91.

[19] A. P. Jia, X. X. Peng, J. X. Qi & X. H. Wu, Numerical study on ship heading stability based on overlapping grid. *Journal of Wuhan Institute of Shipbuilding Technology, 23 (03)*, 2024, 88-91+110.

[20] B. Gao, Z. J. Yan, J. L. Hu, H. Q. Bi, R. Zhang & B. Wu, Study on the influence of freeze-thaw cycles test on the mechanical capacity of insulator. *Insulators and Surge Arresters, (03)*, 2019, 190-196.

[21] P. Zhang, Y. P. Li, W. Wang, T. Q. Ma, M. L. Cai, X. F. Yang & D. M. Zhang, Cement-based compo for porcelain and necessity analysis of standard revision. *Insulators and Surge Arresters, (06)*, 2017, 177-180+186.